



# Comprehensive Analysis of Pyroptosis-Associated in Molecular Classification, Immunity and Prognostic of Glioma

Peng Chen<sup>1</sup>, Yanyan Li<sup>2</sup>, Na Li<sup>3</sup>, Liangfang Shen<sup>3</sup> and Zhanzhan Li<sup>3,4\*</sup>

<sup>1</sup>Department of Orthopedics, Xiangya Hospital, Central South University, Changsha, China, <sup>2</sup>Department of Nursing, Xiangya Hospital, Central South University, Changsha, China, <sup>3</sup>Department of Oncology, Xiangya Hospital, Central South University, Changsha, China, <sup>4</sup>National Clinical Research Center for Geriatric Disorders, Xiangya Hospital, Central South University, Changsha, China

## OPEN ACCESS

### Edited by:

Mehdi Pirooznia,  
National Heart, Lung, and Blood  
Institute (NHLBI), United States

### Reviewed by:

Balaji Banoth,  
St. Jude Children's Research Hospital,  
United States  
Chenghua Li,  
Ningbo University, China

### \*Correspondence:

Zhanzhan Li  
lizhanzhan@csu.edu.cn

### Specialty section:

This article was submitted to  
Computational Genomics,  
a section of the journal  
Frontiers in Genetics

**Received:** 22 September 2021

**Accepted:** 15 December 2021

**Published:** 07 January 2022

### Citation:

Chen P, Li Y, Li N, Shen L and Li Z  
(2022) Comprehensive Analysis of  
Pyroptosis-Associated in Molecular  
Classification, Immunity and  
Prognostic of Glioma.  
*Front. Genet.* 12:781538.  
doi: 10.3389/fgene.2021.781538

Integrative analysis was performed in the Chinese Glioma Genome Atlas and The Cancer Genome Atlas to describe the pyroptosis-associated molecular classification and prognostic signature in glioma. Pyroptosis-related genes were used for consensus clustering and to develop a prognostic signature. The immune statuses, molecular alterations, and clinical features of differentially expressed genes were analyzed among different subclasses and risk groups. A lncRNA-miRNA-mRNA network was built, and drug sensitivity analysis was used to identify small molecular drugs for the identified genes. Glioma can be divided into two subclasses using 30 pyroptosis-related genes. Cluster 1 displayed high immune signatures and poor prognosis as well as high immune-related function scores. A prognostic signature based on 15 pyroptosis-related genes of the CGGA cohort can predict the overall survival of glioma and was well validated in the TCGA cohort. Cluster 1 had higher risk scores. The high-risk group had high immune cell and function scores and low DNA methylation of pyroptosis-related genes. The differences in pyroptosis-related gene mutations and somatic copy numbers were significant between the high-risk and low-risk groups. The ceRNA regulatory network uncovered the regulatory patterns of different risk groups in glioma. Nine pairs of target genes and drugs were identified. *In vitro*, CASP8 promotes the progression of glioma cells. Pyroptosis-related genes can reflect the molecular biological and clinical features of glioma subclasses. The established prognostic signature can predict prognosis and distinguish molecular alterations in glioma patients. Our comprehensive analyses provide valuable guidelines for improving glioma patient management and individualized therapy.

**Keywords:** glioma, pyroptosis, prognostic signature, tumor immunity, clinical nomogram

## INTRODUCTION

Gliomas are the most common types of primary tumors in the central nervous system and one of the most devastating tumors (Weller et al., 2015). At present, the main treatment methods of glioma are surgical resection, radiotherapy, chemotherapy, or chemoradiotherapy (Bush et al., 2017). Although great efforts have been made to improve glioma treatment, the prognosis of glioma patients remains poor (Kan et al., 2020). One of the main reasons is that the molecular mechanism is still not fully

understood. Therefore, the exploration and research of the underlying mechanism of gliomas and identification of potential treatment targets followed by application in clinical practice have important theoretical and practical significance.

Pyroptosis is one of the pathways involved in programmed cell death, such as apoptosis, ferroptosis, necroptosis, and autophagy (Fink and Cookson, 2005). Cookson et al. first used pyroptosis to describe the caspase-1-dependent pattern of cell death found in macrophages (Fink and Cookson, 2006). Pyroptosis, distinct from apoptosis and necrosis, contributes to a range of human diseases as a new mechanism of cell death. Pyroptosis is a proinflammatory form of programmed cell death that is, dependent on the activity of caspase acid-specific proteases (Bergsbaken et al., 2011). In the coupling of the amino-terminal and carboxy-terminal linkers of gasdermin D (GSDMD) by caspases, the latter is displaced onto the membrane and perforated, inducing moisture penetration, cell swelling and the release of inflammatory factors, which is followed by pyroptosis (Boise and Collins, 2001). A previous study reported that pyroptosis plays an important role in immunity and diseases. Pyroptosis can promote the death of damaged cells during infection and acts as an alarm signal for the recruitment of immune cells to the site of infection to promote the removal of pathogens, thus effectively protecting the body (Fink and Cookson, 2019). In recent years, its role in tumorigenesis and cancer development has been studied comprehensively. Various regulators have been reported to be involved in the process of pyroptosis and play pivotal roles in the progression of tumors, such as hepatocellular carcinoma, lung cancer, and breast cancer (Hage et al., 2019; Lu et al., 2020; An et al., 2021). However, few studies have investigated the role of pyroptosis in glioma, and comprehensive analyses of pyroptosis regulators in glioma, their correlation with clinical characteristics and their prognostic value have not been reported.

In the present study, we first outlined the molecular subtypes of gliomas based on pyroptosis-related genes in the CGGA dataset and described the clinical and molecular characteristics and immune status of each subclass. Then, we developed a prognostic signature of pyroptosis-related genes based on the CGGA cohort, validated this prognostic signature in the TCGA cohort. Furthermore, we explored the clinical and molecular patterns, including immune infiltration, somatic copy number alterations, mutations, and DNA methylation, and established a lncRNA-miRNA-mRNA regulatory network. Finally, we explored the correlation between small molecular drugs and the identified prognostic signature genes. Our comprehensive analyses provide new insight into the functions of pyroptosis in the initiation, development, and progression of glioma.

## MATERIALS AND METHODS

### Data Source

We downloaded the genomic data, copy number alteration, methylation and clinical data of glioma patients from the

CGGA (<http://www.cgga.org.cn/>) and TCGA databases (<https://portal.gdc.cancer.gov/>). Additional gene-centric RMA-normalized gene expression profiles and drug response data of over 1000 cancer cell lines were accessed from the Genomics of Drug Sensitivity in Cancer (GDSC) database (<https://www.cancerrxgene.org/downloads>). Immune-associated data, including immune cells and immunophenoscores, were downloaded from TCIA (<https://tcia.at/home>). Thirty-three pyroptosis-related genes were defined from a previous publication and are provided in **Supplementary Table S1** (Man and Kanneganti, 2015; Wang and Yin, 2017; Karki and Kanneganti, 2019; Xia et al., 2019).

### Identification of Glioma Subclasses and Gene Set Variation Analysis

We identified the optimal clustering number visualizing consensus matrix, tracking plot, and cumulative distribution function plot. In addition, a T-distributed stochastic neighbor embedding-based approach was used to validate the clustering in glioma patients. We calculated the enrichment scores for every sample using the GSVA R package.

### Development and Validation of a Prognostic Signature

We developed a pyroptosis-related prognostic signature based on the CGGA training cohort. Twenty differentially expressed genes with  $p < 0.05$  were entered into LASSO Cox regression, which identified potential genes for the prognostic signature in the CGGA training cohort. Then, we calculated the risk score for each sample of the CGGA and TCGA validation cohorts using the obtained regression coefficient in the CGGA training cohort: risk score =  $\text{coef}_1 \times \text{gene}_1 \text{ expression} + \text{coef}_2 \times \text{gene}_2 \text{ expression} + \dots + \text{coef}_n \times \text{gene}_n \text{ expression}$ . The CGGA and TCGA samples were divided into a high-risk group and a low-risk group based on the median risk score. Receiver operating characteristic curves were plotted to evaluate the 1-year, 2-years, and 3-years sensitivity and specificity of the prognostic signature. We also established a prognostic nomogram to evaluate the clinical value of the prognostic signature. Calibration analysis of the prognostic predictive value of the nomogram was carried out.

### Functional Enrichment Analysis, Estimation of Tumor Stem Cell-Like Properties and Immune Infiltration

Gene Ontology and KEGG pathway analyses were performed using the “clusterProfiler” package. We used single-sample gene set enrichment analysis (ssGSEA) to estimate the enrichment score of stem cell-like properties (RNAss, DNAss) and the TME (stromal score, immune score, and ESTIMATE score) in the TCGA cohort because the CGGA dataset did not provide such data. The immune-related cell and function scores were also calculated for each sample (downloaded from <https://www.gsea-msigdb.org/>).



## Somatic Copy Number Alteration, Mutation, and DNA Methylation Analysis

Based on the risk groups in the TCGA cohort, we compared the somatic copy number alteration, mutation, and DNA methylation levels between the high-risk and low-risk groups using the “limma” R package.

## Construction of a ceRNA Network and Drug Sensitivity

To further explore the transcriptome regulation network of different risk groups, we used Cytoscape version 3.8.2 to establish a lncRNA-miRNA-mRNA regulatory network. We explore the correlation between small molecular drugs and the identified prognostic signature genes using Pearson correlation analysis  $|R| > 0.25$  and  $p > 0.05$  were considered significant.

## Verification of Experiments *in Vitro*

We further performed the Western blot, cell migration assays, cell scratchy assays, and clonogenic assays to verify the present finding. We selected the CASP8 to validate the molecular function because CASP8 showed significant differences between normal tissue and GBM or LGG, and the elevated expression is associated with poor prognosis.

The details of experiments process *in vitro* were supplied in **Supplementary Material**.

## Statistical Analysis

The log-rank test was used to compare the survival curves of Kaplan-Meier analysis. The hazard ratio (HR) and 95% confidence interval (CI) of each gene and clinical parameters were calculated when univariate and multivariate Cox regression were applied. All analyses were achieved using R software version 4.0. A two-sided  $p$  value  $< 0.05$  was considered significant unless otherwise specified.

## RESULTS

### Identification of Glioma Subclasses

The flow chart of the data analysis is presented in **Figure 1A**. From two CGGA RNA-seq datasets, we obtained 1018 samples of gene expression data and further identified 30 pyroptosis-related genes based on  $MAD > 0.5$ . The gene symbols and descriptions of the 30 pyroptosis-associated genes used for classification are listed in the **Supplementary Table S1**. We first explored the interactions among these genes using PPIs (**Figure 1B**), and the PPI network indicated that CASP8, CASP4, CASP1, NLRP3, NLRP1, and NLRC4 are hub genes. The correlation circle plot of the 30 genes is presented in **Figure 1C** (red: positive correlation; green: negative correlation). We identified the optimal  $k$  value as 2 by estimating the comprehensive correlation coefficient. Therefore, we divided the glioma samples into two different subclasses: cluster 1 and cluster 2. For the optimal  $k$  value ( $k = 2$ ), the consensus matrix showed a relatively sharp and clear boundary, indicating stable and robust clustering (**Figure 1D**). To verify the subclass stability, we further

performed t-sensitivity PCA and found that a two-dimensional t-sensitivity distribution supported subtype clustering (**Figure 1E**). The consensus clustering for each sample is listed in **Supplementary Table S2**. The Kaplan-Meier analysis indicates that the median survival time was significantly shorter in cluster 2 than in cluster 1 (MST: 1.87 vs. 6.92 years,  $p < 0.001$ , **Figure 1F**). This result indicated that the two subclasses had distinct prognostic patterns.

### Correlation of Glioma Subclasses With Pyroptosis-Related Genes

Two subclasses were obtained based on pyroptosis-related genes. To explore the pathway enrichment for the two subclasses, we performed GSVA by transforming the expression data from a gene-by-sample matrix to a gene set by two subclasses. Then, differential pathways were enriched in the two subclasses. Compared with cluster 1, the GSVA results indicated that cluster 2 had 182 kinds of significantly differential signaling pathways (**Supplementary Table S3**). The upregulated pathways were associated with immune-related pathways, such as autoimmune, allograft rejection, graft vs. host disease, primary immunodeficiency, antigen processing, and presentation. Some signaling pathways, such as the cytosolic DNA sensing pathway, NOD-like receptor signaling pathway, Toll-like receptor signaling pathway, and metabolism-related pathways, were also significantly enriched. The significantly downregulated pathway was long-term potentiation (**Figure 2A**).

### Clinical Characteristics and Transcriptomes of Glioma Subclasses

We explored the correlation of subclasses with clinical characteristics (**Figure 2B**). Compared with patients in cluster 2 with a favorable prognosis, patients in cluster 1 tended to have GBM ( $p < 0.001$ ), WHO grade IV ( $p < 0.001$ ), a higher proportion of age  $> 41$  years, 1p19q non-codeletion status ( $p < 0.001$ ), and IDH wildtype status ( $p < 0.001$ ). Sex, PRS type and radiotherapy status were not associated with the molecular subclasses ( $p > 0.05$ ). For the pyroptosis-related genes except CASP9, significant differential expression was observed in the two clusters. Among these differentially expressed genes, all genes were upregulated in cluster 1 and downregulated in cluster 2 (**Figure 2B**). We also compared the differences in pyroptosis-related genes in patients with different histologies, grades, IDH mutation statuses, and 1p19q statuses. Compared with the LGG group, the GBM group had one upregulated gene (AIM2) and 21 downregulated genes (**Supplementary Figure S1A**). Twenty-one DEGs were found for grade, and their expression increased with increasing WHO grade ( $p < 0.005$ , **Supplementary Figure S1B**). For IDH status, 25 DEGs were found (**Supplementary Figure S1C**). Thirty pyroptosis-related DEGs were found for 1p191 status (**Supplementary Figure S1D**).

We further performed differential expression analysis between cluster 1 and cluster 2. A total of 392 DEGs were found, 18 genes were upregulated, and 372 genes were downregulated in cluster 2 (**Supplementary Table S4**). GO and KEGG enrichment analyses

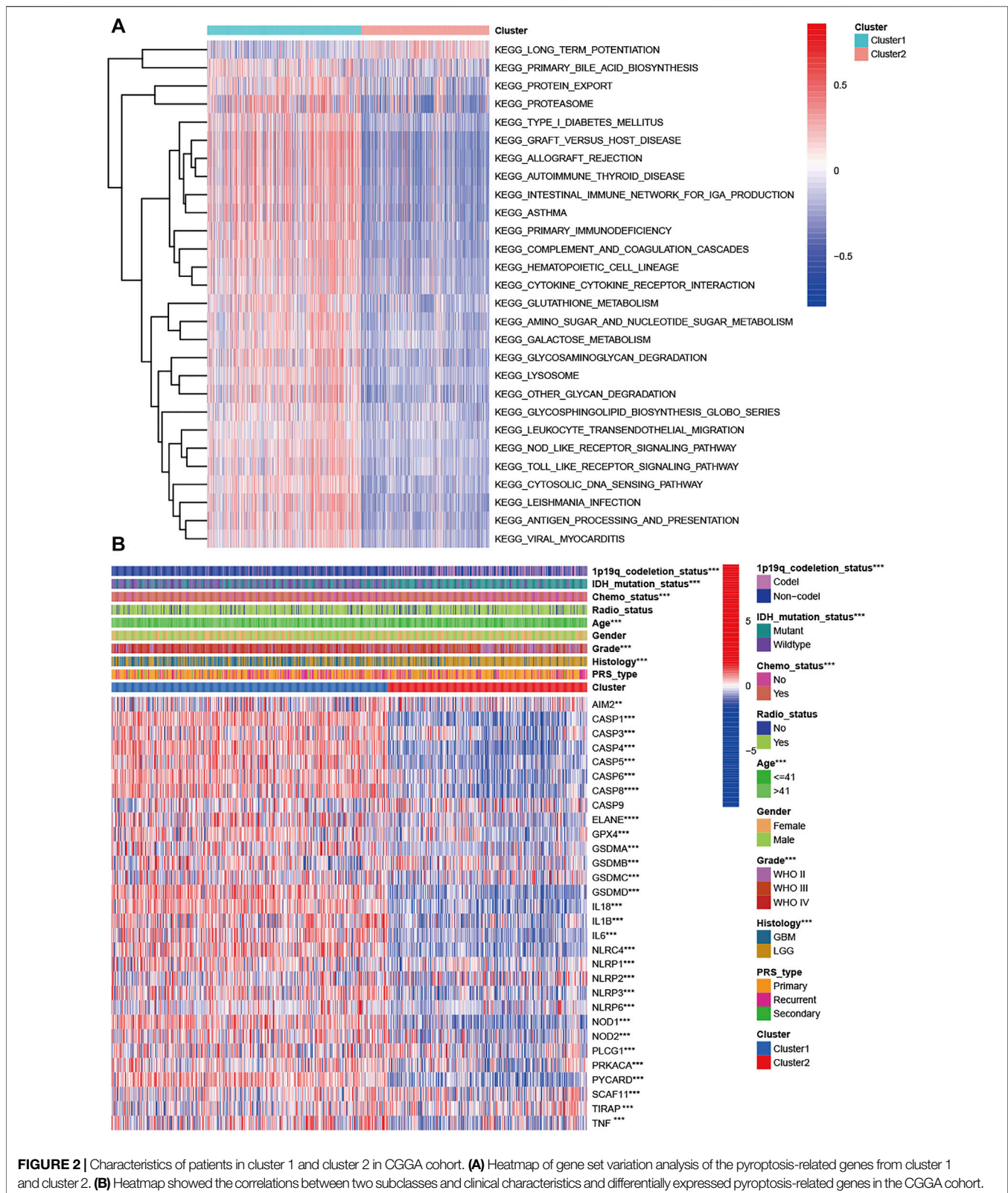


**FIGURE 2 |** Characteristics of patients in cluster 1 and cluster 2 in CGGA cohort. **(A)** Heatmap of gene set variation analysis of the pyroptosis-related genes from cluster 1 and cluster 2. **(B)** Heatmap showed the correlations between two subclasses and clinical characteristics and differentially expressed pyroptosis-related genes in the CGGA cohort.

were performed for all DEGs (**Supplementary Tables S5, S6**). A total of 874 differentially expressed functions were enriched, including 709 biological processes, 95 cellular components and

70 molecular functions. The top 30 enrichment results are presented in **Supplementary Figure S2**. Most of these functions were associated with immunity. In addition, 56

pathways were also identified in the KEGG analysis (**Supplementary Figure S3**), and the top five pathways were phagosome, *Staphylococcus aureus* infection, tuberculosis, complement and coagulation cascades, and human T-cell leukemia virus 1 infection.

## Correlation of Glioma Subclasses With Immune Status

To explore the tumor heterogeneity between the two subclasses, we investigated the immune cell and immune function differences. Compared with cluster 2, cluster 1 had higher aDC, CD8<sup>+</sup> T cell, DC, iDC, macrophage, mast cell, neutrophil, NK cell, pDC, T helper cell, Tfh cell, Th2 cell, TIL, and Treg levels (all  $p < 0.001$ , **Supplementary Figure S4A**). Similarly, cluster 1 had higher immune function scores than cluster 2, including APC coinhibition, APC costimulation, CCR, checkpoint, cytolytic activity, HLA, inflammation promotion, MHC class I, parainflammation, T cell coinhibition, type I IFN response and type II IFN response (all  $p < 0.001$ , **Supplementary Figure S4B**).

## Development of a Pyroptosis-Related Prognostic Signature in Glioma

Initially, we performed univariate Cox regression to identify the correlations of the 30 pyroptosis-related genes with OS (**Supplementary Figure S5A**) in the CGGA cohort. In total, 20 pyroptosis-related genes were identified as associated with the overall survival of glioma patients. The Kaplan-Meier plot indicated that high expression of CASP3, CASP4, CASP5, CASP6, CASP8, ELANE, GSMAD, IL6, NLRP3, NOD1, NOD2, PLCG1, PRKACA, PYCARD, and SCAF11 was associated with poorer OS in glioma. Using 20 prognostic pyroptosis-related genes, we developed a prognostic signature by performing LASSO regression in the CGGA training cohort (**Supplementary Figures S5B,C**). Fifteen of the 20 prognostic genes were used to develop the risk signature. We calculated the risk score for each sample using the regression coefficients of the 15 genes (**Supplementary Table S7**). Glioma patients with risk scores greater than the median value were divided into a high-risk group, and the others were divided into a low-risk group. Compared with the low-risk group, the high-risk group was more likely to have GBM ( $p < 0.001$ ), a higher WHO grade ( $p < 0.001$ ), recurrence ( $p < 0.001$ ), older age ( $p < 0.001$ ), IDH wildtype status ( $p < 0.001$ ), 1p19q non-codeletion status ( $p < 0.001$ ), and a history of chemotherapy ( $p < 0.001$ ). The heatmap showed the association between the risk group and clinical parameters and differentially expressed genes of the high- and low-risk groups (**Supplementary Figure S5D**). Furthermore, we found that glioma patients belonging to cluster 1, patients with a poor prognosis, patients with GBM, patients with WHO grade IV patients with 1p19q non-codeletion status and patients with IDH wildtype status had higher risk scores (all  $p < 0.001$ , **Supplementary Figure S6**).

The Kaplan-Meier analysis showed that the high-risk group had a significantly poorer OS than the low-risk group (**Figures**

**3A,B**). Univariate Cox regression indicated that the risk score was positively associated with OS in glioma (HR = 3.105, 95% CI: 2.681–3.596,  $p < 0.001$ , **Figure 3C**). Multivariate Cox regression suggested that the risk score was an independent unfavorable prognostic predictor in glioma (HR = 1.685, 95% CI: 1.392–2.039,  $p < 0.001$ , **Figure 3D**). In addition, PRS type, tumor grade, and age were positively associated with OS. However, chemotherapy, wildtype IDH status, and 1p19q status were negatively associated with OS in the CGGA training cohort. The PCA plot indicated that patients in different risk groups were separated into obviously different clusters (**Figure 3E**). Time-dependent receiver operating characteristic analysis was performed to evaluate the predictability of the prognostic model. Our results showed that the AUCs at 1, 2, and 3 years were 0.717, 0.784, and 0.773 (**Figure 3F**), respectively. We further compared the OS status among different histology, IDH status, 1p19q codeletion status, and grade subgroups. The results showed that the OS of the high-risk group was still poorer than that of the low-risk group (**Supplementary Figure S7**, all  $p < 0.001$ ).

## External Validation of the Pyroptosis-Related Prognostic Signature in Glioma

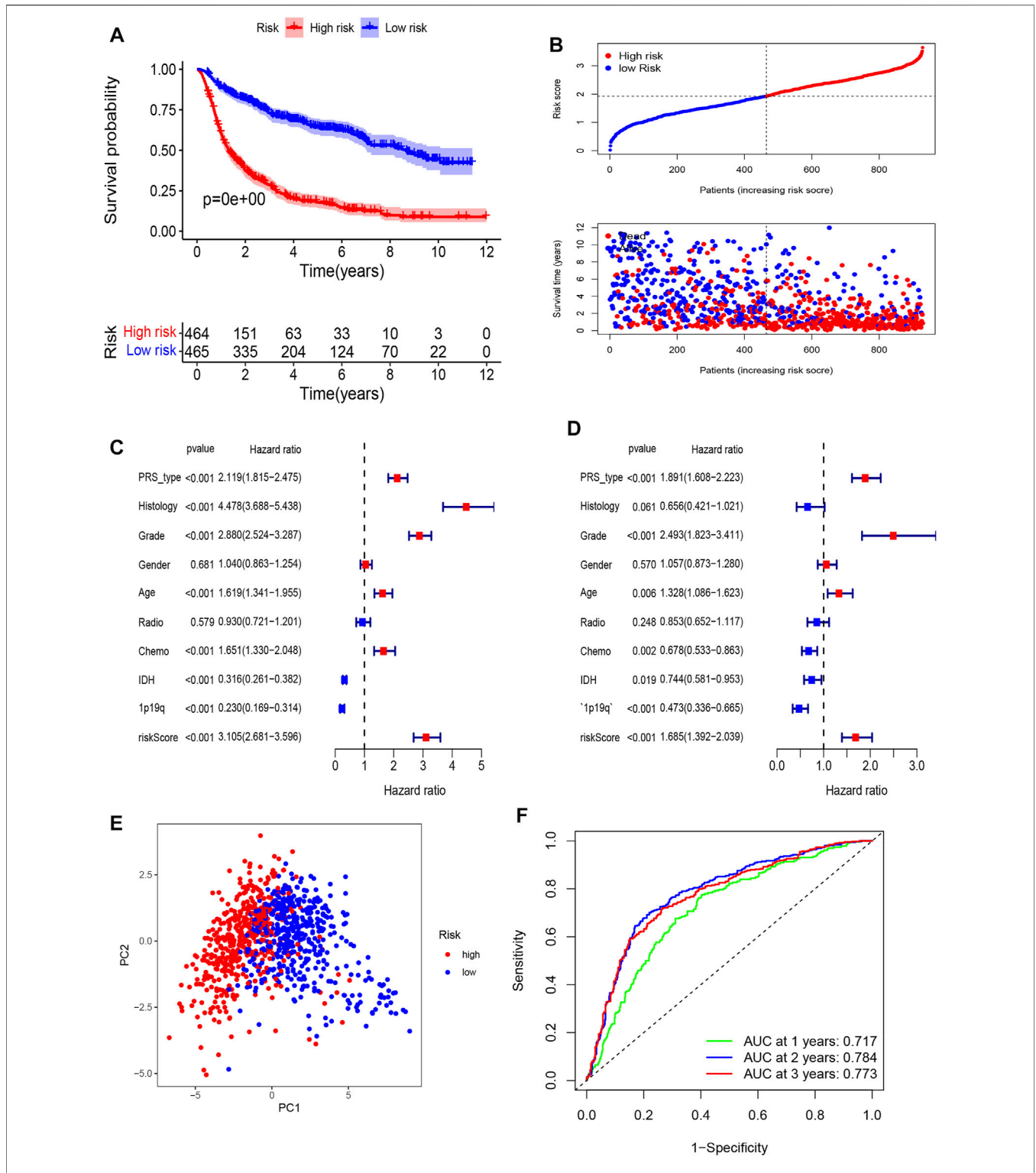
To further validate the prognostic value of the pyroptosis-related gene model, we also calculated the risk score of glioma patients in the TCGA cohort using the regression coefficients of the CGGA cohort. The Kaplan-Meier analysis indicated a significant correlation of the high-risk group with worse OS than the low-risk group (**Figures 4A–C**). Univariate Cox regression showed that the risk score was significantly associated with OS in the TCGA cohort (HR = 2.084, 95% CI: 1.890–2.297,  $p < 0.001$ , **Figure 4D**). In multivariate Cox regression, the risk score was also an independent prognostic indicator (HR = 1.425, 95% CI: 1.247–1.629  $p < 0.001$ , **Figure 4E**). The PCA plot validated the high- and low-risk distribution of all glioma patients based on the TCGA cohort. Furthermore, the AUCs of the risk score were 0.844 at 1 year, 0.863 at 2 years, and 0.874 at 3 years (**Figure 4F**).

## Prognostic Prediction Models

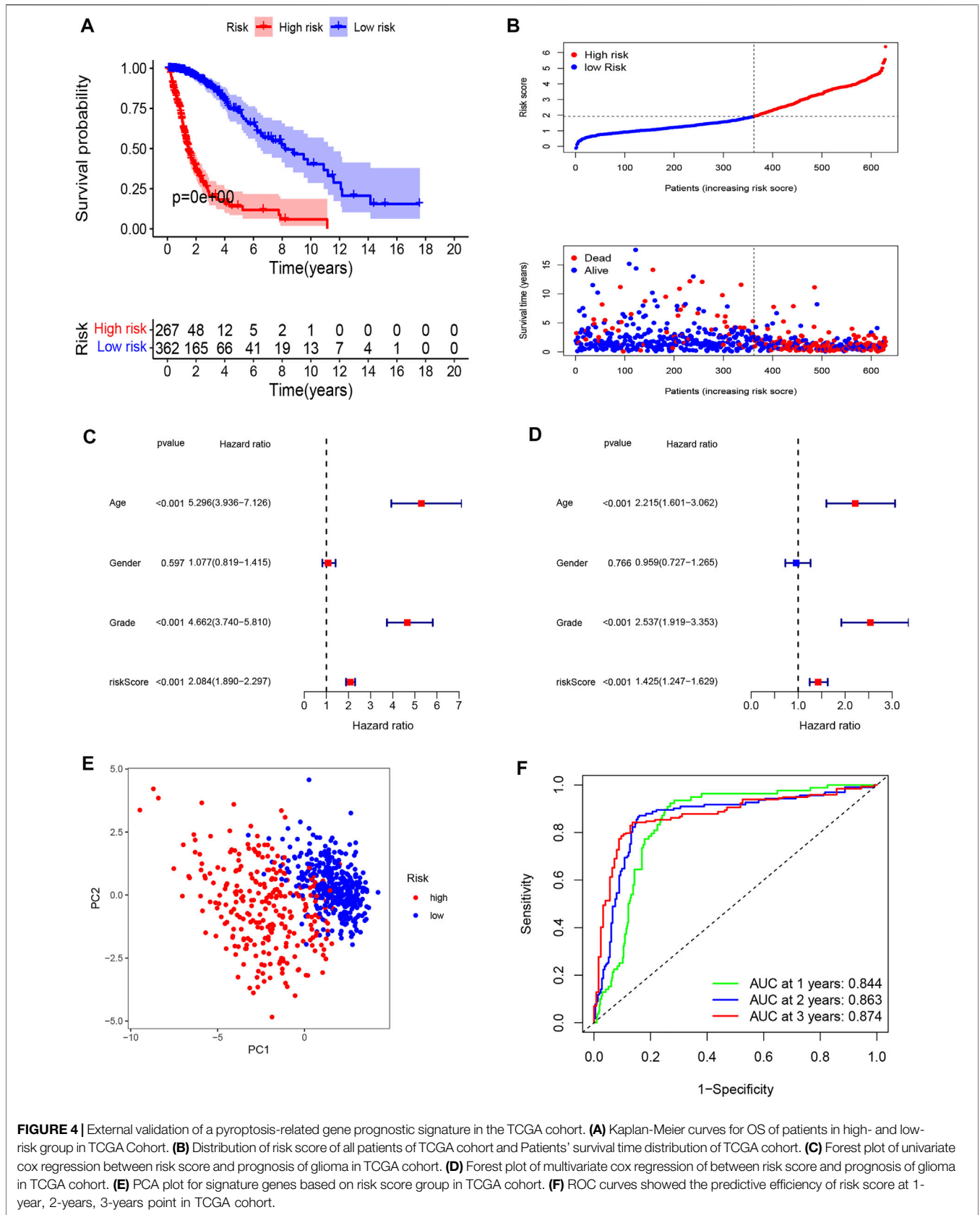
To further evaluate the clinical prediction value of the prognostic signature, we constructed a prognostic nomogram model based on multivariate Cox regression analysis that included all clinical parameters in the CGGA cohort. The calibration curves indicated that the clinical nomogram model could precisely predict the 1, 3, and 5-years OS of glioma patients (C-index = 0.799). The predictive accuracy of this nomogram was well validated in the TCGA cohort (C-index = 0.841, **Figure 5**).

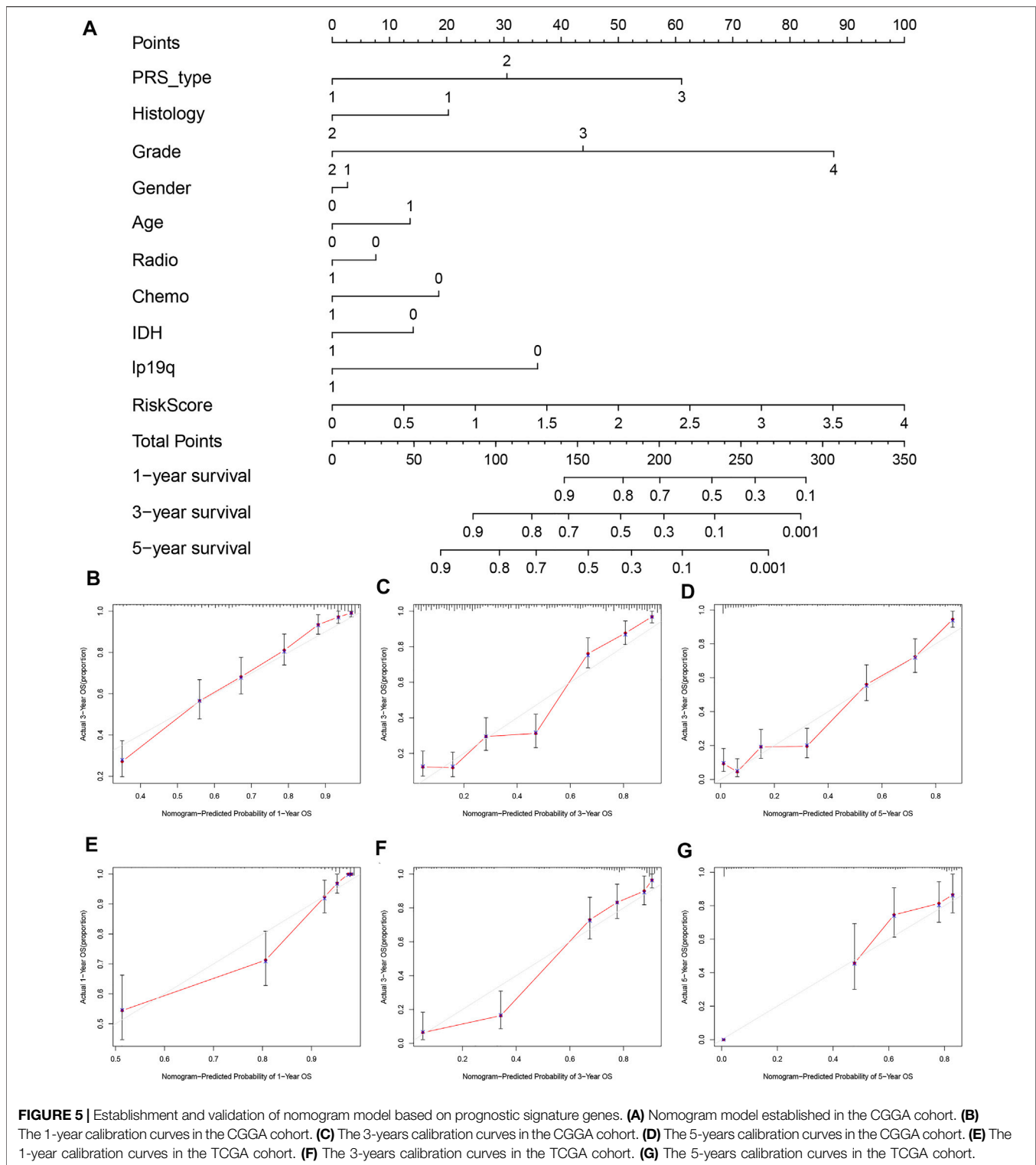
## Functional Enrichment and Immune Infiltration Analyses Based on the Prognostic Signature

We further explored the underlying biological functions that define the survival of glioma patients. We first performed



**FIGURE 3 |** Establishment of a pyroptosis-related gene prognostic signature in the CGGA cohort. **(A)** Kaplan-Meier curves for OS of patients in high- and low-risk group in CGGA Cohort. **(B)** Distribution of risk score of all patients of CGGA cohort, and Patients' survival time distribution. **(C)** Forest plot of univariate cox regression between risk score and prognosis of glioma. **(D)** Forest plot of multivariate cox regression of between risk score and prognosis of glioma. **(E)** PCA plot for signature genes based on risk score group. **(F)** ROC curves showed the predictive efficiency of risk score at 1-year, 2-years, 3-years point.





DEG analysis between the high-risk and low-risk groups and then annotated the functions of the DEGs in terms of biological processes, cellular components, and molecular functions using GO enrichment and KEGG pathways. We identified 338 DEGs in

the CGGA cohort (**Supplementary Table S8**) and 2600 DEGs in the TCGA cohort (**Supplementary Table S9**). The GO enrichment and KEGG pathway analyses indicated that the CGGA and TCGA cohorts shared some enrichment results,

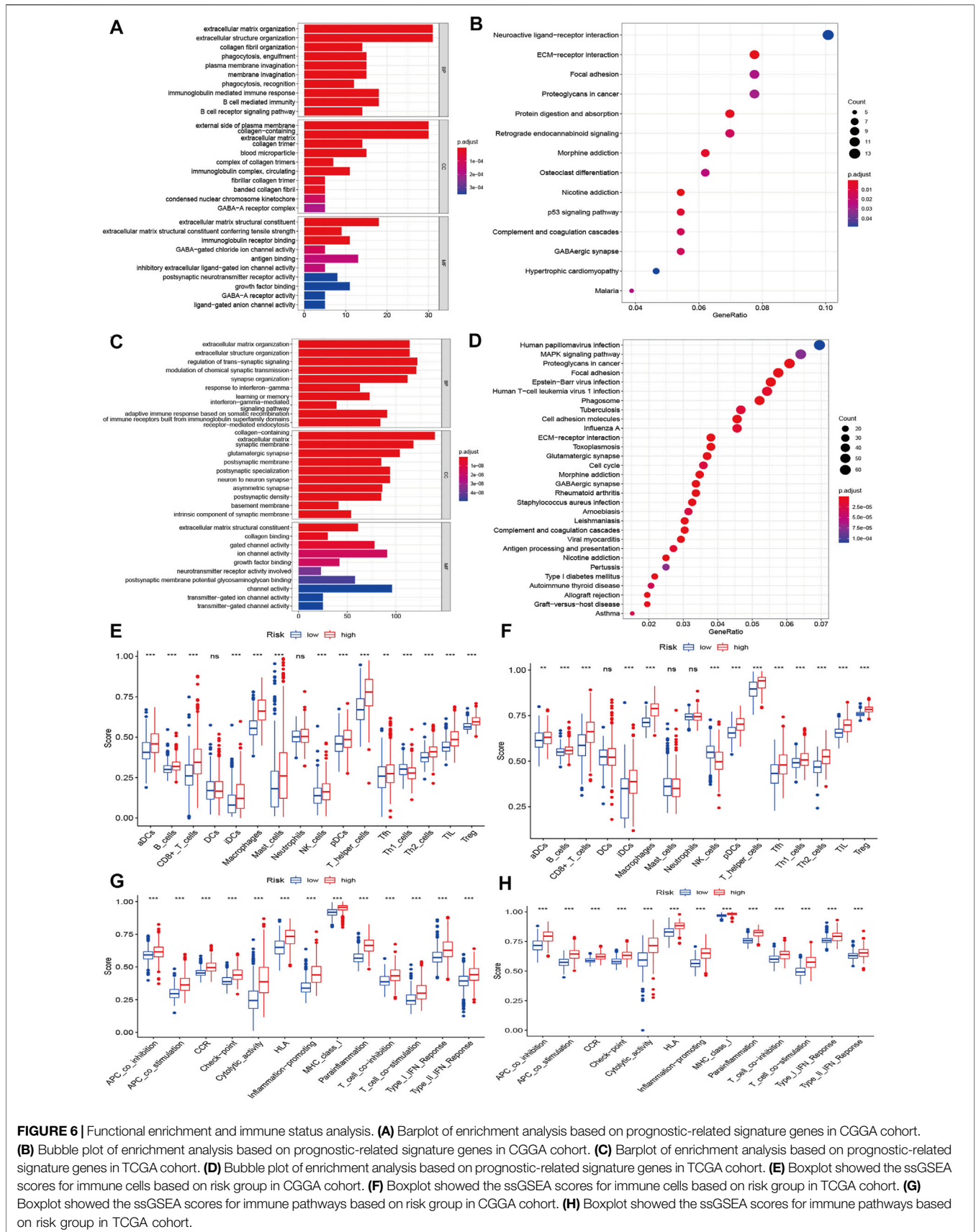


**FIGURE 6 |** Functional enrichment and immune status analysis. **(A)** Barplot of enrichment analysis based on prognostic-related signature genes in CGGA cohort. **(B)** Bubble plot of enrichment analysis based on prognostic-related signature genes in CGGA cohort. **(C)** Barplot of enrichment analysis based on prognostic-related signature genes in TCGA cohort. **(D)** Bubble plot of enrichment analysis based on prognostic-related signature genes in TCGA cohort. **(E)** Boxplot showed the ssGSEA scores for immune cells based on risk group in CGGA cohort. **(F)** Boxplot showed the ssGSEA scores for immune cells based on risk group in TCGA cohort. **(G)** Boxplot showed the ssGSEA scores for immune pathways based on risk group in CGGA cohort. **(H)** Boxplot showed the ssGSEA scores for immune pathways based on risk group in TCGA cohort.

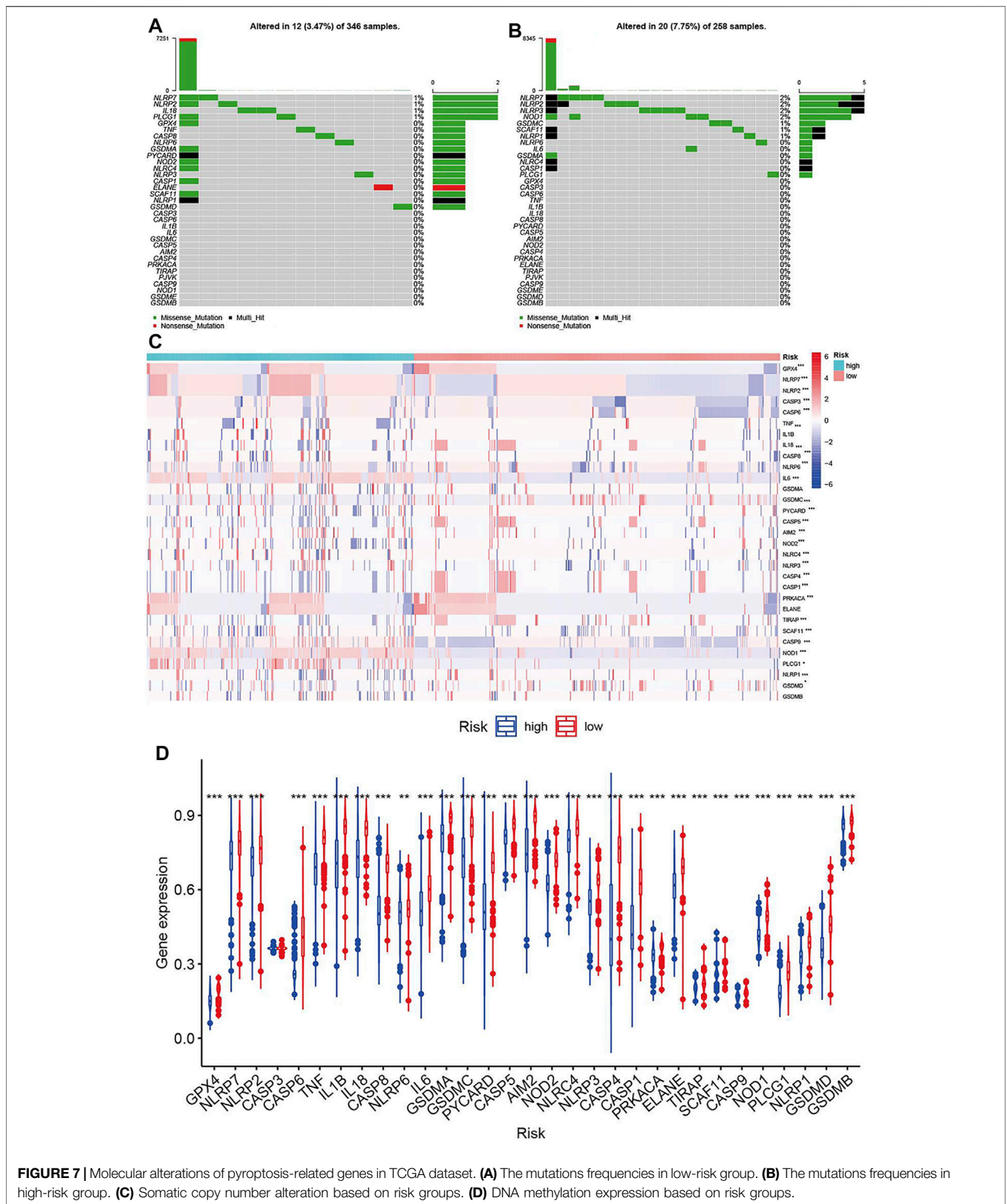


**FIGURE 7 |** Molecular alterations of pyroptosis-related genes in TCGA dataset. **(A)** The mutations frequencies in low-risk group. **(B)** The mutations frequencies in high-risk group. **(C)** Somatic copy number alteration based on risk groups. **(D)** DNA methylation expression based on risk groups.

such as extracellular matrix organization, extracellular structure organization, immune response, ECM-receptor interaction, and cell adhesion molecules (**Figures 6A–D**).

We also explored the differences in immune cells and immune functions based on the risk score in the CGGA (**Figures 6E,G**) and TCGA datasets (**Figures 6F,H**). As shown in the box plots, the immune cell score showed a similar trend in the CGGA and TCGA datasets. All immune cell scores were significantly upregulated in the high-risk group. The immune function differences of the different risk groups were the same in the CGGA and TCGA datasets (all  $p < 0.001$ ). All immune function scores were significantly upregulated in the high-risk group. Significant expression levels were also observed among different immune subtypes, which indicated that the glioma prognosis risk could be associated with immune status (**Supplementary Figure S8**). We also explored the correlation of the expression of target genes with cancer stem cell-like properties (RNAss, DNAss) and the TME (stromal score, immune score, and ESTIMATE score). We found that PCG1 was negatively associated with RNAss, the stromal score, the immune score, and the ESTIMATE score. SCAF11 was only negatively associated with DNAss. The rest of the genes showed positive correlations with RNAss, DNAss and the stromal, immune and ESTIMATE scores (**Supplementary Figure S9**).

## Molecular Alterations of Pyroptosis-Related Genes Based on the Prognostic Signature

Molecular alterations of pyroptosis-related genes were also evaluated based on histology in the TCGA dataset. NLRP2, NLRP7, and PLCG1 were the only gene alterations in LGG, and NLRP3, NLRP7, NLRP2, SCAF11, NOD1, PLCG1, NLRP1, and CASP1 were gene alterations in GBM. All gene alterations were within 2% (**Figure 7**). The somatic copy number alteration analysis indicated significant differences among the pyroptosis-related genes. Among these genes, the copy variation number was significantly increased in GPX4, NLRP7, NLRP2, CASP3, CASP6, IL1B, CASP8, IL6, AIM2, NLRP4, NLRP3, PRKACA, ELANE, SCAF11, CASP9, NOD1, and PLCG1 and was significantly decreased in GSDMB, GSDMD, NLRP1, CASP9, TIRAP, CASP1, CASP4, NOD2, CASP5, PYCARD, GSDMD, GSDMA, and IL18 in the high-risk group. The DNA methylation levels of the pyroptosis-related genes were also compared. The results showed that the overall DNA methylation levels were significantly decreased in the high-risk group and increased in the low-risk group.

## Construction of a ceRNA Network Based on the Prognostic Signature

A ceRNA network was constructed based on the differentially expressed mRNAs, lncRNAs and miRNAs between the high-risk and low-risk groups in the TCGA dataset. We identified 763 downregulated mRNAs, 1176 upregulated mRNAs, 116 downregulated lncRNAs, 132 upregulated lncRNAs (**Supplementary Table S10**), 47 downregulated miRNAs and 71 upregulated miRNAs (**Supplementary Table S11**). Finally, 39

mRNAs (28 upregulated and 11 downregulated), 26 lncRNAs (15 upregulated and 15 downregulated) and 14 miRNAs (13 upregulated and 1 downregulated) were included in the ceRNA network (**Figure 8**). The Kaplan-Meier curves suggested that 13 lncRNAs (positive correlation: AC025211.1, AC068643.1, GDNF-AS1, and LINC00519; negative correlation: ADH1L1-AS2, CRNDE, FAM181A-AS1, HOTAIRM1, MCF2L-AS1, MIR210HG, NEAT1, SLC6A1, and SNHG9; **Supplementary Figure S10**), 41 mRNAs (**Supplementary Table S12**, **Supplementary Figure S11**) and 8 miRNAs (miR-21, miR-155, miR-200a, miR-216a, miR-221, miR-222, miR-429, and miR-503; **Supplementary Figure S12**) were associated with OS in glioma patients.

## Drug Sensitivity Analysis

To identify potential target drugs, we performed correlations of the identified prognostic signature genes with drugs. We identified 257 pairs of significant gene-drug correlations (**Supplementary Table S13**). There were 9 pairs with correlation coefficients  $>0.5$  or  $<-0.5$ .

ELANE-hydroxyurea, ELANE-cyclophosphamide, CASP3-nelarabine, NOD2-imiquimod, NLRP3-rebimastat, ELANE-ABT-199, ELANE-imexon, and NOD2-isotretinoin showed drug sensitivity. PRKACA-cobimetinib showed drug resistance (**Figure 9**).

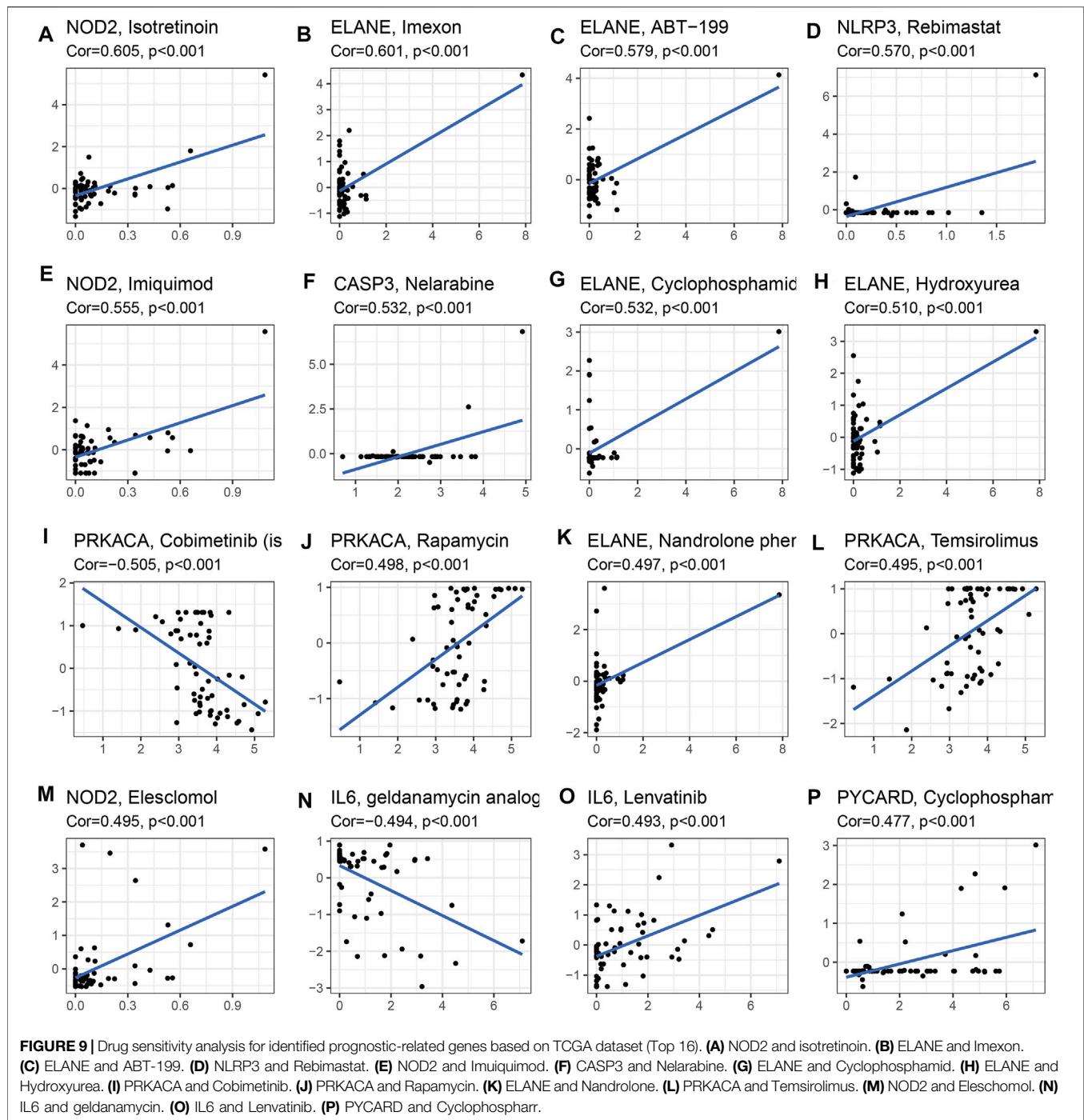
## CASP8 Promotes the Progression of Glioma Cells

We selected the CASP8 to validate the molecular function because: First, the significantly high expression of CASP8 is found between glioma and normal control (**Supplementary Figure S16**). Second, CASP8 is included the prognosis model based on pyroptosis-related genes (**Supplementary Table S7**). Third, the elevated expression of CASP8 is more significantly associated with poor overall survival (**Supplementary Table S7**). We firstly detected the expression of CASP8 in glioma cell lines using the Western blot analysis, and found CASP8 is the most highly expressed in LN299 cell. We built the CASP8-si LN229, H4 and U87 cells of glioma. The qPCR indicated mRNA level of CASP8 is significantly down-regulated in U87 and LN229 cells. Furthermore, the silence of CASP8 expression inhibited the cell migration ability (**Figure 10**). The clonogenic assay also showed that the number of clonogenicity of U87 and LN229 cells were significantly suppressed after knockout of CASP8. These results suggested that CASP8 promotes the progression of glioma cells.

## DISCUSSION

The traditional histologic-based classification has some limitations, although this classification system has been updated several times over the years and serves clinicians well. One of the primary limitations is interobserver variability (Chen et al., 2017). A previous study reported that the concordance for reviewing a case is only approximately 50% among different neuropathologists, especially for astrocytic glioma versus





the cytoplasm necessary for the occurrence of inflammation and can recognize dangerous signaling molecules such as bacteria and viruses. The inflammasome is mainly composed of pattern recognition receptors (PRRs), apoptosis-associated speck-like protein (ASC) and pro-caspase-1 precursors (Platnich and Muruve, 2019). PRRs are receptor proteins responsible for recognizing different signal stimuli in cells. They are mainly composed of nucleotide-binding oligomerization domain-like receptor protein (NLRP) 1, NLRP3, nucleotide-binding

oligomerization domain-like receptor protein C4 (NLRC4), absent in melanoma 2 (AIM2) and other components (Man and Kanneganti, 2015). ASC is an adaptor protein that is, mainly composed of the N-terminal pyrin domain (PYD) and the C-terminal caspase activation and recruitment domain (CARD) (Nambayan et al., 2019). Caspase-1 is an effector molecule that can specifically cleave GSDMD after activation. After the danger signal sensor NLR1, NLRP3 or AIM2 recognizes the danger signal molecule, the N-terminal PYD is combined with

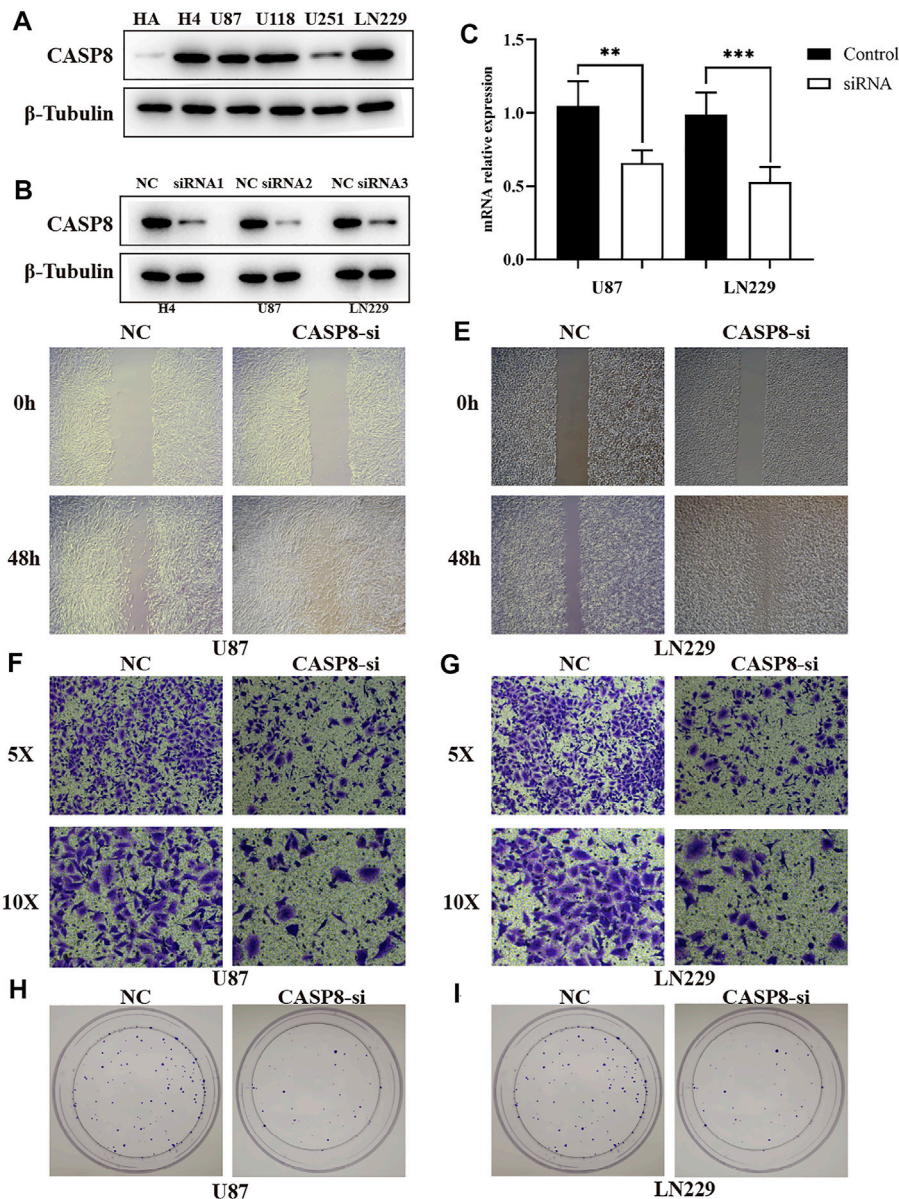


**FIGURE 10 |** CASP8 promotes progression of glioma cells. **(A)** The expression of CASP8 protein in human HA and glioma cell lines. **(B)** The western blot of CASP8 in U87, U1251, H4 cell lines after siRNA. **(C)** The mRNA expression level of CSAP8 in U87 and U251 after siRNA. **(D, E)** The scratch assay of CASP8-si in U87 and U251 cell lines. **(F, G)** Transwell assay of CASP8-si U87 and U251 cell lines. **(H, I)** The clonogenic assay of CASP8 in U87 and U251 cell lines.

the N-terminal PYD of the adaptor protein. ASC then recruits Caspase-1 through the interaction of the CARD domain to complete the assembly of the inflammasome (Lu et al., 2014). This method of cell death mediated by Caspase-1 is called the classical pathway of pyroptosis (Case and Roy, 2013). The non-classical pathway of pyrolysis is mainly mediated by Caspase-4, Caspase-5, and Caspase-11. After cells are stimulated by bacterial LPS, Caspases-4, -5, and -11 directly bind to bacterial LPS and are activated (Lagrange et al., 2018). Activated Caspases-4, -5, and -11 specifically cleave GSDMD and release the intramolecular inhibition of the GSDMD-N domain (Shi et al., 2015). The combination of the GSDMD-N-terminus and cell membrane

phospholipids causes cell membrane pore formation, cell swelling and rupture and induces cell pyrolysis; the GSDMD-N-terminus can also activate Caspase-1 by activating the NLRP3 inflammasome (Kayagaki et al., 2015). Activated Caspase-1 promotes the maturation of IL-18 and IL-1 $\beta$  precursors, and IL-18 and IL-1 $\beta$  are secreted to the outside of the cell and amplify the inflammatory response. Yang et al. found that in the nonclassical pathway that relies on Caspase-11, gap junction protein-1 (Pannexin-1) can be cleaved, and the cleavage of Pannexin-1 can activate its own channel and release ATP, which induces pyrolysis (Yang et al., 2015). Lamkanfi et al. found that in the nonclassical pathway that relies on Caspase-

11, Pannexin-1 cleavage can also activate the NLRP3 inflammasome, which in turn activates Caspase-1 and induces the occurrence of pyroptosis (Lamkanfi and Dixit, 2014). According to the results, mutations of pyroptosis-related genes are mainly attributed to the classical pathway of pyrolysis. More research is needed to validate the molecular mechanisms.

Based on the risk score, we classified glioma patients into high- and low-risk groups to discriminate clinical outcomes. We further explored the molecular features between the high- and low-risk groups. The functional enrichment analysis results were similar in the TCGA and CGGA datasets, and the same pathways appeared in the two datasets, such as ECM-receptor interaction, GABAergic synapse, focal adhesion, and extracellular matrix organization. The immune cells and immune functions showed similar trends: immune cell and functional scores were higher in the high-risk group. The clinical features showed that cluster 1 had a higher risk score and poorer prognosis than cluster 2. The results indicated that the classification was accurate and validated in the risk model. Furthermore, we compared the gene alterations, CNVs, and DNA methylation levels. Significantly different levels were observed, which reflected the different molecular features of the different risk groups. To explore the regulation mechanism of pyroptosis-related genes in glioma, we constructed a ceRNA network. The ceRNA network identified several key lncRNA-miRNA-mRNA regulatory networks: FAM181A-AS1-miR-21-(CPEB3, SAIB1, BLC7A, MAP2K3, JAG1, TGFBI, FAM46A, SPRY2, and CALD1). The survival analysis further suggested the regulatory correlation: elevated FAM181A-AS1 and miR-21 were associated with poor prognosis in glioma, and low expression of BCL7A, SATB1, and CPEB3 was associated with favorable prognosis. Previous experiments have reported the promoting role of miR-21 in glioma (Hermansen et al., 2016), and upregulation of SATB1 and CPEB3 is associated with the development and progression of glioma (Chu et al., 2012; He et al., 2021). These results suggested that the FAM181A-AS1-miR-21-SATB1/CPEB3 axis may be one of molecular mechanisms for glioma progression. Because this regulation network is based on high- and low-risk groups of pyroptosis-related genes risk model score, which means this regulation network may tend to explain the mechanisms of different risk groups. The experiments validations were required for this regulation network. The drug sensitivity analysis indicated that NOD2, ELANE, CASP3, and PYCARD showed sensitivity to small molecular drugs, and PRKACA, IL6, and NLLRP3 showed resistance to some drugs. It was reported that the inhibition of the NLRP3 inflammasome by beta-hydroxybutyrate can suppress the migration of glioma cells (Shang et al., 2018). These results may provide some guidelines for clinical practice. *In vitro*, we found that CASP8 promotes the progression of glioma cells. CASP8 has been shown to be involved in pyroptosis in recent years but also has a role in apoptosis processes. However, our data indicated that higher CASP8 expression is found in glioma than control, the expression is highest in WHO IV, WHO III takes second place, and WHO II is the lowest, and the elevated CASP8 is associated with poor

overall survival. These results indicate that CASP8 may play an oncogene role in glioma.

Sum it up, the pyroptosis-related genes can be used for molecular subtyping and predicting prognosis in glioma. The differences of genes alterations, immune infiltration, and stem cell-like properties chime with the different risk groups based on risk scores of pyroptosis-related genes, which were also involved in complicated lncRNA-miRNA-mRNA regulatory networks in glioma. Our study provides a new understanding of pyroptosis in the development and progression of glioma and contributes new important insights for promoting glioma treatment strategies.

## DATA AVAILABILITY STATEMENT

The original contributions presented in the study are included in the article/**Supplementary Material**, further inquiries can be directed to the corresponding author.

## ETHICS STATEMENT

Ethical approval was not provided for this study on human participants because the data is from public data. The ethics committee waived the requirement of written informed consent for participation. Written informed consent was not obtained from the individual(s) for the publication of any potentially identifiable images or data included in this article.

## AUTHOR CONTRIBUTIONS

ZL designed this study and directed the research group in all aspects, including planning, execution, and analysis of the study. LS drafted the manuscript. YL, NL, and PC collected the data. ZL provided the statistical software, performed the data analysis, YL arranged the Figures and Tables. LS revised the manuscript. All authors have read and approved the final version of the manuscript.

## FUNDING

This study was supported by the National Natural Science Foundation of China (No. 82003239), Hunan Province Natural Science Foundation (Youth Foundation Project) (NO. 2019JJ50945), and the Science Foundation of Xiangya Hospital for Young Scholar (NO. 2018Q012).

## SUPPLEMENTARY MATERIAL

The Supplementary Material for this article can be found online at: <https://www.frontiersin.org/articles/10.3389/fgene.2021.781538/full#supplementary-material>

## REFERENCES

- An, H., Heo, J. S., Kim, P., Lian, Z., Lee, S., Park, J., et al. (2021). Tetraarsenic Hexoxide Enhances Generation of Mitochondrial ROS to Promote Pyroptosis by Inducing the Activation of Caspase-3/GSDME in Triple-Negative Breast Cancer Cells. *Cell Death Dis* 12, 159. doi:10.1038/s41419-021-03454-9
- Bergsbaken, T., Fink, S. L., den Hartigh, A. B., Loomis, W. P., and Cookson, B. T. (2011). Coordinated Host Responses during Pyroptosis: Caspase-1-dependent Lysosome Exocytosis and Inflammatory Cytokine Maturation. *J. Immunology* 187, 2748–2754. doi:10.4049/jimmunol.1100477
- Boise, L. H., and Collins, C. M. (2001). Salmonella-induced Cell Death: Apoptosis, Necrosis or Programmed Cell Death. *Trends Microbiol.* 9, 64–67. doi:10.1016/s0966-842x(00)01937-5
- Bush, N. A. O., Chang, S. M., and Berger, M. S. (2017). Current and Future Strategies for Treatment of Glioma. *Neurosurg. Rev.* 40, 1–14. doi:10.1007/s10143-016-0709-8
- Case, C. L., and Roy, C. R. (2013). Analyzing Caspase-1 Activation during *Legionella pneumophila* Infection in Macrophages. *Methods Mol. Biol.* 954, 479–491. doi:10.1007/978-1-62703-161-5\_29
- Chen, R., Smith-Cohn, M., Cohen, A. L., and Colman, H. (2017). Glioma Subclassifications and Their Clinical Significance. *Neurotherapeutics* 14, 284–297. doi:10.1007/s13311-017-0519-x
- Chu, S.-H., Ma, Y.-B., Feng, D.-F., Zhang, H., Zhu, Z.-A., Li, Z.-Q., et al. (2012). Upregulation of SATB1 Is Associated with the Development and Progression of Glioma. *J. Transl Med.* 10, 149. doi:10.1186/1479-5876-10-149
- Coons, S. W., Johnson, P. C., Scheithauer, B. W., Yates, A. J., and Pearl, D. K. (1997). Improving Diagnostic Accuracy and Interobserver Concordance in the Classification and Grading of Primary Gliomas. *Cancer* 79, 1381–1393. doi:10.1002/(sici)1097-0142(19970401)79:7<1381:aid-cnrc16>3.0.co;2-w
- Fink, S. L., and Cookson, B. T. (2005). Apoptosis, Pyroptosis, and Necrosis: Mechanistic Description of Dead and Dying Eukaryotic Cells. *Infect. Immun.* 73, 1907–1916. doi:10.1128/IAI.73.4.1907-1916.2005
- Fink, S. L., and Cookson, B. T. (2006). Caspase-1-dependent Pore Formation during Pyroptosis Leads to Osmotic Lysis of Infected Host Macrophages. *Cell Microbiol* 8, 1812–1825. doi:10.1111/j.1462-5822.2006.00751.x
- Fink, S. L., and Cookson, B. T. (2019). Caspase-1-dependent Pore Formation during Pyroptosis Leads to Osmotic Lysis of Infected Host Macrophages. *Cell Microbiol.* 2006. 8: 1812-1825. *J. Immunol.* 202, 1913–1926. doi:10.1111/j.1462-5822.2006.00751.x
- Giordanella, G., Motta, C., Muriana, S., Arena, V., Anuso, C. D., Lupo, G., et al. (2011). Cytosolic and Calcium-independent Phospholipase A2 Mediate Glioma-Enhanced Proangiogenic Activity of Brain Endothelial Cells. *Microvasc. Res.* 81, 1–17. doi:10.1016/j.mvr.2010.11.005
- Hage, C., Hoves, S., Strauss, L., Bissinger, S., Prinz, Y., Pöschinger, T., et al. (2019). Sorafenib Induces Pyroptosis in Macrophages and Triggers Natural Killer Cell-Mediated Cytotoxicity against Hepatocellular Carcinoma. *Hepatology* 70, 1280–1297. doi:10.1002/hep.30666
- He, Y., Nan, H., Yan, L., Ma, T., Man, M., Tian, B., et al. (2021). Long Non-coding RNA MIR22HG Inhibits Glioma Progression by Downregulating microRNA-9/CPEB3. *Oncol. Lett.* 21, 157. doi:10.3892/ol.2020.12418
- Hermansen, S. K., Nielsen, B. S., Aaberg-Jessen, C., and Kristensen, B. W. (2016). miR-21 Is Linked to Glioma Angiogenesis. *J. Histochem. Cytochem.* 64, 138–148. doi:10.1369/0022155415623515
- Huang, Y., Zhang, Q., Lubas, M., Yuan, Y., Yalcin, F., Efe, I. E., et al. (2020). Synergistic Toll-like Receptor 3/9 Signaling Affects Properties and Impairs Glioma-Promoting Activity of Microglia. *J. Neurosci.* 40, 6428–6443. doi:10.1523/JNEUROSCI.0666-20.2020
- Kan, L. K., Drummond, K., Hunn, M., Williams, D., O'Brien, T. J., and Monif, M. (2020). Potential Biomarkers and Challenges in Glioma Diagnosis, Therapy and Prognosis. *BMJ Neurol. Open* 2, e000069. doi:10.1136/bmjno-2020-000069
- Karki, R., and Kanneganti, T.-D. (2019). Diverging Inflammasome Signals in Tumorigenesis and Potential Targeting. *Nat. Rev. Cancer* 19, 197–214. doi:10.1038/s41568-019-0123-y
- Kayagaki, N., Stowe, I. B., Lee, B. L., O'Rourke, K., Anderson, K., Warming, S., et al. (2015). Caspase-11 Cleaves Gasdermin D for Non-canonical Inflammasome Signalling. *Nature* 526, 666–671. doi:10.1038/nature15541
- Lagrange, B., Benaoudia, S., Wallet, P., Magnotti, F., Provost, A., Michal, F., et al. (2018). Human Caspase-4 Detects Tetra-Acylated LPS and Cytosolic Francisella and Functions Differently from Murine Caspase-11. *Nat. Commun.* 9, 242. doi:10.1038/s41467-017-02682-y
- Lamkanfi, M., and Dixit, V. M. (2014). Mechanisms and Functions of Inflammasomes. *Cell* 157, 1013–1022. doi:10.1016/j.cell.2014.04.007
- Lu, A., Magupalli, V. G., Ruan, J., Yin, Q., Atianand, M. K., Vos, M. R., et al. (2014). Unified Polymerization Mechanism for the Assembly of ASC-dependent Inflammasomes. *Cell* 156, 1193–1206. doi:10.1016/j.cell.2014.02.008
- Lu, C., Guo, C., Chen, H., Zhang, H., Zhi, L., Lv, T., et al. (2020). A Novel Chimeric PD1-Nkg2d-41bb Receptor Enhances Antitumor Activity of NK92 Cells against Human Lung Cancer H1299 Cells by Triggering Pyroptosis. *Mol. Immunol.* 122, 200–206. doi:10.1016/j.molimm.2020.04.016
- Man, S. M., and Kanneganti, T.-D. (2015). Regulation of Inflammasome Activation. *Immunol. Rev.* 265, 6–21. doi:10.1111/imr.12296
- Nambayan, R. J. T., Sandin, S. I., Quint, D. A., Satyadi, D. M., and de Alba, E. (2019). The Inflammasome Adapter ASC Assembles into Filaments with Integral Participation of its Two Death Domains, PYD and CARD. *J. Biol. Chem.* 294, 439–452. doi:10.1074/jbc.RA118.004407
- Platnich, J. M., and Muruve, D. A. (2019). NOD-like Receptors and Inflammasomes: A Review of Their Canonical and Non-canonical Signaling Pathways. *Arch. Biochem. Biophys.* 670, 4–14. doi:10.1016/j.abb.2019.02.008
- Saxena, S., and Jha, S. (2017). Role of NOD-like Receptors in Glioma Angiogenesis: Insights into Future Therapeutic Interventions. *Cytokine Growth Factor. Rev.* 34, 15–26. doi:10.1016/j.cytogfr.2017.02.001
- Shang, S., Wang, L., Zhang, Y., Lu, H., and Lu, X. (2018). The Beta-Hydroxybutyrate Suppresses the Migration of Glioma Cells by Inhibition of NLRP3 Inflammasome. *Cell Mol Neurobiol* 38, 1479–1489. doi:10.1007/s10571-018-0617-2
- Shi, J., Zhao, Y., Wang, K., Shi, X., Wang, Y., Huang, H., et al. (2015). Cleavage of GSDMD by Inflammatory Caspases Determines Pyroptotic Cell Death. *Nature* 526, 660–665. doi:10.1038/nature15514
- Wang, B., and Yin, Q. (2017). AIM2 Inflammasome Activation and Regulation: A Structural Perspective. *J. Struct. Biol.* 200, 279–282. doi:10.1016/j.jsb.2017.08.001
- Wang, Q., Wang, Y., Ding, J., Wang, C., Zhou, X., Gao, W., et al. (2020). A Bioorthogonal System Reveals Antitumor Immune Function of Pyroptosis. *Nature* 579, 421–426. doi:10.1038/s41586-020-2079-1
- Weller, M., Wick, W., Aldape, K., Brada, M., Berger, M., Pfister, S. M., et al. (2015). Glioma. *Nat. Rev. Dis. Primers* 1, 15017. doi:10.1038/nrdp.2015.17
- Xia, X., Wang, X., Cheng, Z., Qin, W., Lei, L., Jiang, J., et al. (2019). The Role of Pyroptosis in Cancer: Pro-cancer or Pro-"host". *Cell Death Dis* 10, 650. doi:10.1038/s41419-019-1883-8
- Yang, D., He, Y., Muñoz-Planillo, R., Liu, Q., and Núñez, G. (2015). Caspase-11 Requires the Pannexin-1 Channel and the Purinergic P2X7 Pore to Mediate Pyroptosis and Endotoxic Shock. *Immunity* 43, 923–932. doi:10.1016/j.immuni.2015.10.009

**Conflict of Interest:** The authors declare that the research was conducted in the absence of any commercial or financial relationships that could be construed as a potential conflict of interest.

**Publisher's Note:** All claims expressed in this article are solely those of the authors and do not necessarily represent those of their affiliated organizations, or those of the publisher, the editors and the reviewers. Any product that may be evaluated in this article, or claim that may be made by its manufacturer, is not guaranteed or endorsed by the publisher.

Copyright © 2022 Chen, Li, Shen and Li. This is an open-access article distributed under the terms of the Creative Commons Attribution License (CC BY). The use, distribution or reproduction in other forums is permitted, provided the original author(s) and the copyright owner(s) are credited and that the original publication in this journal is cited, in accordance with accepted academic practice. No use, distribution or reproduction is permitted which does not comply with these terms.